Article
JOURNAL OF UNIVERSITY OF BABYLON
For Pure and Applied Sciences (JUBPAS)
Vol. ; No. | 2024

Employing HSOFM Neural Network and FCM To Extract Liver's Abnormal Regions In MRI and CT Scan Images

[1]Rabab Saadoon Abdoon [2]E. A. Salman [*3]Reem Tuama Yousif [4]S. T. Salman [5]A. A. Hussein

[1]College of Science, University of Babylon, sci.rabab.saadoon@uobabylon.edu.iq, Iraq.
[2]Musayyib General Hospital, abdrabab1@gmail.com , Iraq.
[3]College of Science, University of Babylon, sci.reem.taumu@uobabylon.edu.iq , Iraq.
[4]College of Science, University of Babylon, suha.t.alshaban@gmail.com , Iraq.
[5]College of Science, University of Babylon, sci970.asyl.ali@uobabylon.edu.iq , Iraq.
*Corresponding author email: sci.reem.taumu@uobabylon.edu.iq

Accepted: 4/8/2025 **Published:** 30/9/2025

ABSTRACT

Background: A Liver tumor is a dangerous disease that may leads to death, the chances of survival will increase when it is detected in early time.

Materials and Methods: In this study, clustering Fuzzy c-mean and "Self-Organization Feature Map", HSOFM, which is an unsupervised artificial neural network, based on the histogram of the image, are presented for segmenting, isolating, and then extracting tumors and other abnormal regions in liver images of MRI and CT imaging. In an additional processing, morphological operations were used to achieve the complete final extraction of the isolated regions without any extra pixels that do not belong to the abnormal regions. These two methods were applied on five MRI and four CT scan images. The extracted regions surface areas were calculated and compared with the groundtruth, manually extracted mass regions, to check the goodness adequacy of the adopted methods. The work was achieved by Mat Lab programing environment.

Results: The percent relative differences of the extracted abnormal regions by implementing the adopted methods with the groundtruth were ranged from 1.108 % to 3.861 % for the images of MRI, while for CT scan images, the percent relative differences were in the range from 0.732 % to 3.456%. By implementing FCM clustering, the percent relative difference ranged from 0.724% to 4.370 % for three MRI images, while for CT scan images, the percent relative difference was 4.327 % for one of the adopted CT images. Results of implementing HSOFM indicate the high-quality performance of this method with 95 % accuracy.

Conclusion: From the results we can conclude that there is an appropriate number of nodes and clusters that is a more adequate choice than others depending on the properties' intensity variance in each processed image. The comparison between the two implemented methods figures out the superiority of the HSOFM method over FCM. There are some limitations, such as the small size of the abnormal regions as well as the interference of the abnormal regions with the normal regions of the similar intensity that require applying advanced enhancement methods as an additional preprocessing step.

Key words: **liver abnormalities, FCM, HSOFM, MRI, CT.**

ISSN: 2312-8135 | Print ISSN: 1992-0652
info@journalofbabylon.com | jub@itnet.uobabylon.edu.iq | www.journalofbabylon.com

ISSN: 2312-8135 | Print ISSN: 1992-0652
info@journalofbabylon.com | jub@itnet.uobabylon.edu.iq | www.journalofbabylon.com

1.INTRODUCTION

The Liver is a big organ located at the upper right side within the abdomens. It occupies a large region in the medical images of the abdomen [1]. The Liver is consisting of different cell types. The Liver cells are: hepatocytes cells and bile ducts. The bile ducts carry the bile from liver externally to the gallbladder or directly to the intestines. All the liver cell types may be susceptible to many different types of tumors and to other types of lesions [2].

Liver malignant tumor is the fifth most widespread cancer. It carries a low survival rate [3]. Nevertheless, early detection of cancers and presenting effective treatment strategies can enhance the overall survival rate [4].

Many medical scanning modalities are principal ways for early and fast diagnosis of the existence of cancer, lesions and other abnormalities within any part or organ within the body [5]. These types of imaging are: x-rays; computed tomography, (CT scan); magnetic resonance imaging, (MRI); mammography; IR thermography; PET; SPECT and many others. In this study, MRI and CT imaging type images were adopted to detect liver abnormalities. MRI considers a non-invasive technique for scanning the internal structures and certain aspects of function inside the body. MRI uses radio frequency waves with a controlled magnetic field. It does not use ionizing radiation which makes it one of the safest imaging techniques available. MRI scans is utilized to scan any part of the body, providing fine detailed information; they present the changes between different types of tissue in a good way [6].

Due to the importance of revealing tumors and other liver lesions, many researchers presented their works in image processing for segmenting the medical images of the liver to determine sites, areas, volumes and the abnormal regions shapes, besides any other important information to assist getting an accurate diagnosis. Many segmenting approaches were offered to perform this job, and most of these methods were equivalent giving promising results [5,7]. Some of these studies employed clustering methods to segment the medical images, while others suggested methods based on the texture. Besides, others adopted ‘artificial neural network’ methodologies and many other approaches, as in these references [1, 3-5, 8-17]. In this study, we employed HSOFM "an unsupervised clustering artificial neural network", and FCM algorithm, with the aid of different morphological operations for segmenting purposes and to extract the abnormal regions in five MRI and four CT scan liver images. In addition, FCM" unsupervised fuzzy clustering method" was implemented, and its results were compared with the results of HSOFM. This work was achieved with the aid of the programing MatLab environment.

ISSN: 2312-8135 | Print ISSN: 1992-0652
info@journalofbabylon.com | jub@itnet.uobabylon.edu.iq | www.journalofbabylon.com

2. ARTIFICIAL NEURAL NETWORK (ANN)

Artificial neural networks (ANN) can be considered as parallel networks of many cells, textual elements, or central nodes that simulate the biological learning and make preliminary calculations. By adapting the weights of the links between nodes, learning is achieved. Artificial neural networks are widely used in medical scanning for classification (this means that training data is weighted and then the artificial neural network is used to divide new data, and this type of training is called the "supervised method"). Additionally, ANNs can be used as a "clustering technique" in an unsupervised manner. [18]. The inspiration behind the advancement of neural network knowledge arose from the need to develop an artificial system capable of achieving intelligent tasks similar to those accomplished by the human brain. ANNs imitate the Haman brain in two ways: Neural networks gain knowledge through learning and store the knowledge by learning processes and storing what was learned within the strengths of communication between neurons known as synaptic weights. The real strength and usefulness of neural networks lies in their ability to represent linear and non-linear relationships and in their ability to learn these relationships directly from the modeled data [19].

In this study, artificial neural networks of un-supervised training approach were used. The network starting with training process of the dataset to adopting the outcome to classify the input data. At this point, the "test input data" classification is achieved once the network has been trained on a particular dataset. Classification is adopted at this stage. The assembly process is achieved through this kind of ANN. In cases of aggregation, ANN collects observations in two main steps. In the first step, the learning base is used to train the network on an accurate dataset. This step is called a training or learning step. In the second step, notes are classified, and this step is called the reminder step. ANNs work with layers: the input layer consists of the nodes through which the data are entered. The output layer produces output that the user can interpret. There can be other layers between these two layers which are called (hidden layers). The output of each layer is an input of the next layer until the reference reaches the output layers. [20]. (Self-Organization Feature Map, SOFM) SOFM works by a feed-forward process, and this neural network is employed to segment medical images. In its procedure, SOFM is different compared with other ANN in the sense that they utilized a neighborhood function to reserve the " topological characteristics" of the input image space [21]. The technique of employing a vector from the data space on the map is to catch the closest node that possesses a weight vector to the vector from the data space and allocate this node's map coordinates to that vector. For all weight vectors, Euclidean distance is assessed. The "best match unit'', (BMU) label is given to the neurons with a weight vector that is closer to the input one. The BMU's weights and the following next neurons in the network are modified to be as the input vector. The value of the change reduces with both distance and time from the BMU. The updating formula for the neuron of some weight vector can be written as [22]:

$$\mathbf{w_i\ (t+1) = w_i\ (t)+\alpha(t)\ h_{ci}\ (t)(x(t)-w(t))} \quad \ldots\ldots\ldots\ldots\ldots\ldots\ldots\ldots(1)$$

In which, $w_i(t)$ is the weight given to input x_i, α(t) is a coefficient of the monotonically decreasing learning, and $h_{ci}(t)$ represents the neighborhood function, it is considered as a Gaussian function. The process is repeated a very large number of iterations. SOFM

ISSN: 2312-8135 | Print ISSN: 1992-0652 | info@journalofbabylon.com | jub@itnet.uobabylon.edu.iq | www.journalofbabylon.com

preserves the significant metric and topological relations of the primary data items. SOFM is employed to partition the medical images [23, 24].

In this work, SOFM based on the highest peaks of the processed image histogram to get the most adequate results and we called this technique histogram based SOFM,' HSOFM '.

3.FUZZY C-MEAN (FCM) ALGORITHM

FCM clustering method is a clustering process of an unsupervised approach; it usually applied to solve many problems like feature analysis clustering and classifier design. This algorithm, FCM, adopts the partial membership of each image pixel intensity and it manipulates the image data, so that FCM method belongs to fuzzy logic. In FCM, there are Blur (uncertain) groups and its algorithm is a grouping that allows a single piece of data to belong to more than one blur group. As a result, the intermediate values that is a member of one blur group are also a members of other blur groups in the same image but with different values of the membership. FCM algorithm is a method of grouping that allows a single piece of data to belong to more than one group. By FCM algorithm, the data set is clustered into number of groups, say ***n*** groups and each point in the data set is belongs to each group to a certain extent. In the FCM, a point that lies far from the center of mass will have a low degree of membership in that group. Another point is that point located near the center of mass will have a high degree of membership in that group. The centers of mass start with an initial guess in order to determine each group's average location [25]. This algorithm requires a large memory to gather the big data so that it may take a long time to apply FCM [26].

To gather pixels into one group exclusively approaches of hard grouping are used. However, FCM allows points in more than one group based on grades of the membership, the membership sum of each point in the given data sets must be equal. Let X = {x_1, x_2, x_3..., x_n} be the set of the data pixels and C = {c_1, c_2, c_3..., c_n} be the centers of the data set. The value of the update membership and center of the cluster for each iteration are presented in Equations (2) and (3) [27,28].

$$\mu_{ij} = \frac{1}{\sum_{k=1}^{c} \left(\frac{dij}{dij}\right)^{\left(\frac{1}{(m-1)}\right)}} \quad \ldots. \quad (2)$$

$$c_j = \sum_{i=1}^{n} \left(\frac{(u\,ij)^m\, xi)}{(u\,ij)^m}\right) \ldots. (3)$$

where d_{ij} represents the distance between the i^{th} data and the j^{th} center, c represents the clusters' number, while m refers to the fuzziness index, μ_{ij} represents the membership of the i data to the center of mass j, n is the number of data points and cj represents the mass center j^{th}

FCM method may preserve more information from the original image than hard segmenting algorithms. The basic FCM objective function for dividing a dataset *Xk* N(K=1) into c clusters is defined mathematically by. As show in Equations (4) and (5) [29]:

$$J_M = \sum_{i=1}^{c} \sum_{K=1}^{N} u_{ik}^{m} \, \|Xk - vi\|^2 \ldots. (4)$$

ISSN: 2312-8135 | Print ISSN: 1992-0652
info@journalofbabylon.com | jub@itnet.uobabylon.edu.iq | www.journalofbabylon.com

where $\{v\}_{i=1}^{c}$ are the centers or prototypes of the clusters and the array $\{u_{ik}\}$= (U) represents a partition matrix satisfying

$$U \in \{uik \in [0,1] | \sum_{i=1}^{c} uik = 1, \forall k \text{ and } 0 < \sum_{K=1}^{N} u_{ik} < N, \forall i\} \ldots (5)$$

The parameter m is a fuzzy membership weighting exponent that controls the level of fuzziness in the resultant classification. When high membership values are awarded to pixels whose intensities are near to the centroid of their respective class and low membership values are assigned when the pixel data is distant from the centroid FCM objective function is minimized [29].

4. MORPHOLOGICAL OPERATIONS

Morphological operators are usually utilized in the image processing field. They are desired because of their strong achievement in maintaining the signal shape, while submitting the noise [30]. The morphology of the image provides a manner to join neighborhood and distance information into algorithms. The basic idea of the mathematical morphology is that it convolves an image with a specified mask denoted as a structuring element and binarizes the result of the convolution using a specified function. The selection of the convolution mask and the binarization function is subject to the specific morphological operator being used [31]. Erosion and Dilation conceder the two essential morphological operations. Opening and Closing are two processes derived from erosion and dilation. In the dilation process, pixels are added to the boundaries of objects in the processed image, while erosion eliminates pixels on the boundaries of the object. The number of pixels that are added or eliminated from objects in an image depends on the selected size and shape of the structuring element [32].

5. Materials and Methods

The main steps of this work are illustrated in Fig. (1). This work was achieved with the aid of the programing MatLab environment.

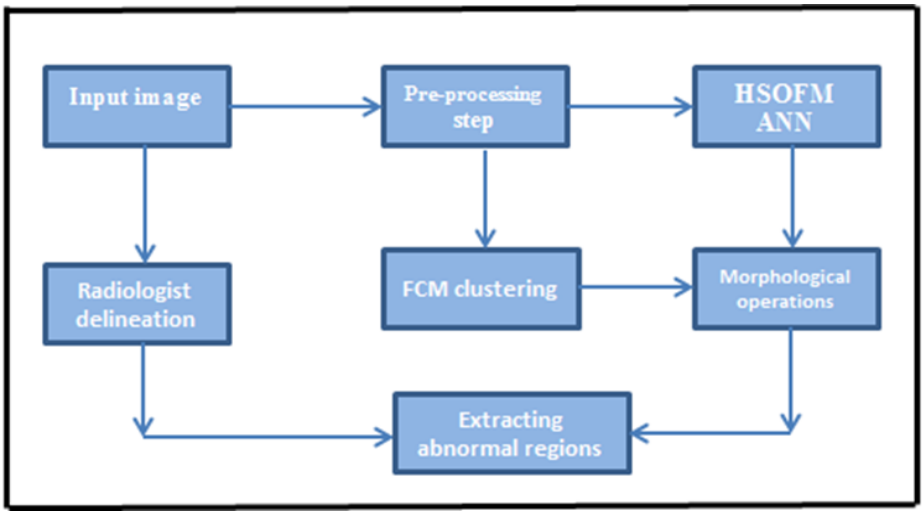

Fig. (1): Block diagram of the work (in the current study).

ISSN: 2312-8135 | Print ISSN: 1992-0652
info@journalofbabylon.com | jub@itnet.uobabylon.edu.iq | www.journalofbabylon.com

The under study images are medical liver images are five MRI and four CT scan images which were acquired from Iraqi local clinic/ Iraq. Fig. (2) shows the images under study and Table (1) presents the most important information of these adopted images.

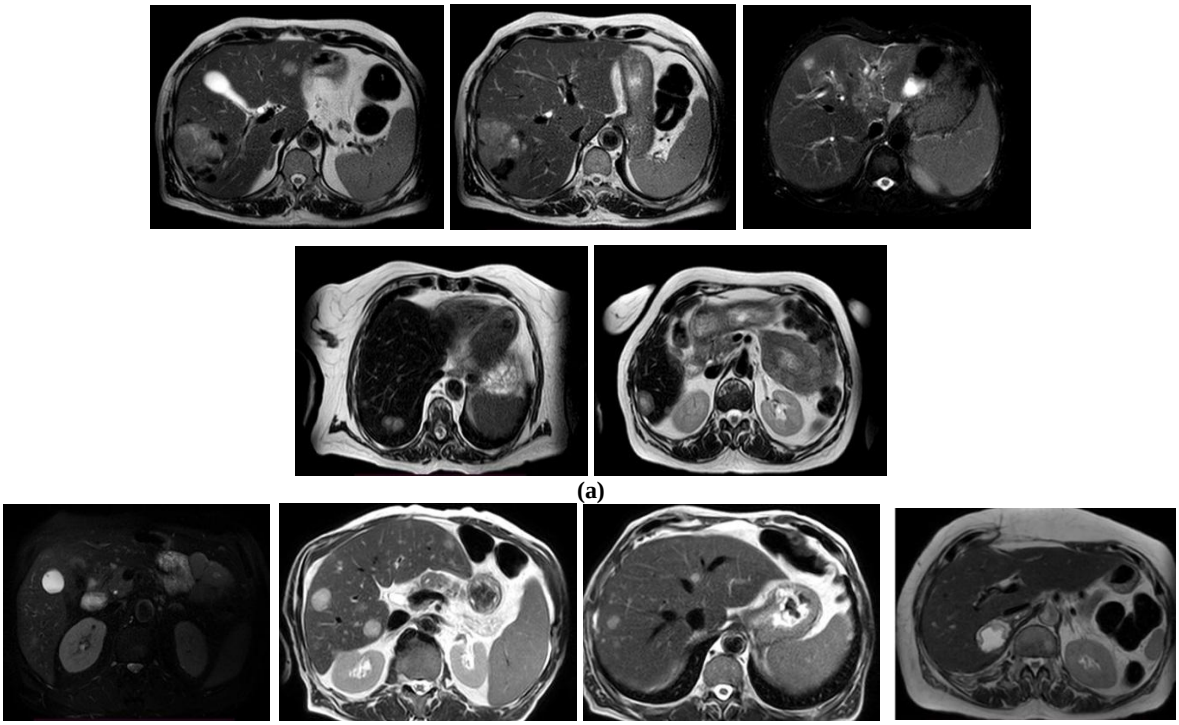

(a)

(b)

Fig. (2): The input images: (a) MRI and (b) CT (in the current study**).**

ISSN: 2312-8135 | Print ISSN: 1992-0652
info@journalofbabylon.com | jub@itnet.uobabylon.edu.iq | www.journalofbabylon.com

Table (1): The most important information of the adopted images.

Image	Name of image	Modality	Size of images (pixels)	Abnormality and Tumor type	Source
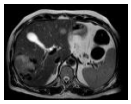	Im1	MRI	640x640	Multiple hemangioma	Clinical Medical imaging Center in Hilla/Iraq
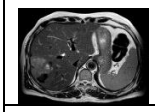	Im2		640x6404	Multiple hemangioma	
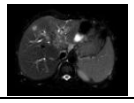	Im3		640x640	cholangiocarcinoma+ Liver secondaries	
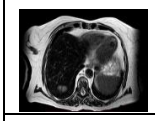	Im4		470x707	Liver metastasis	
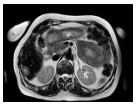	Im5		465x675	Liver metastasis	
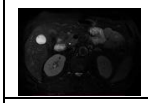	Im11	CT	399 x568	Hydatid cyst	
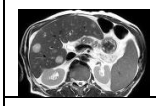	Im22		367x561	Liver secondaries	
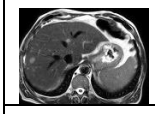	Im33		372x506	Liver secondaries	
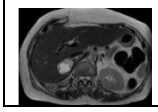	Im44		675x896	Hydatid cyst	

ISSN: 2312-8135 | Print ISSN: 1992-0652
info@journalofbabylon.com | jub@itnet.uobabylon.edu.iq | www.journalofbabylon.com

6. RESULTS

The results of implementing HSOFM method on the liver images under study are presented as follows:

6.1 MRI images

HSOFM was implemented on MRI images, that named **Im1**, **Im2, Im3, Im4** and **Im5,** with different number of nodes to figur out the most proper number of nodes. The following figures presente the results of clustering and segmenting the adopted images with 5, 6 and 7 nodes for one image as an example .

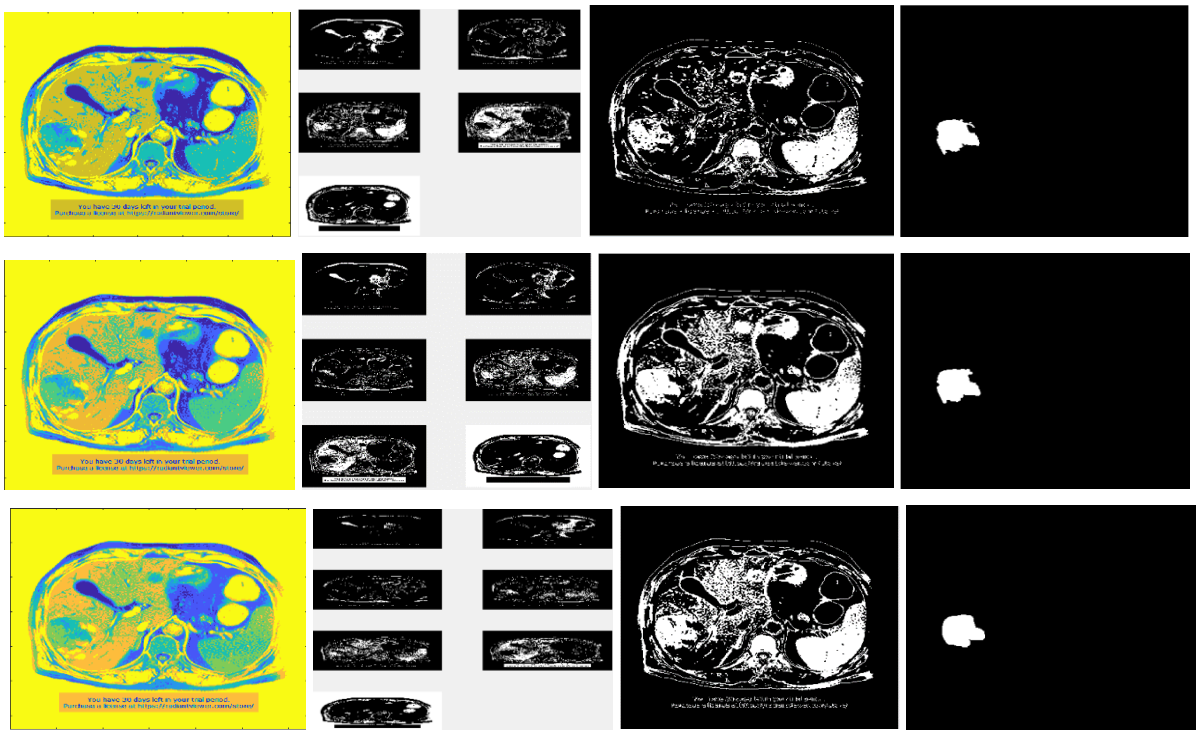

Fig. (3): The results HSOFM net on Im1 image with five, six and seven nodes. (a) segmented image, (b) discrete segments, (c) abnormality segment and (d) final refined extracted abnormality area (in the current study**).**

The results of segmenting the rest four images are presented in Fig. (4), where the first line of images shows the input images **Im2**, **Im3**, **Im4** and **Im5** from left to right respectively, second one is for the corresponding segmented images by adopting five number of nodes, third one for six number of nodes and the last one is for the segmented images by adopting seven number of nodes.

ISSN: 2312-8135 | Print ISSN: 1992-0652
info@journalofbabylon.com | jub@itnet.uobabylon.edu.iq | www.journalofbabylon.com

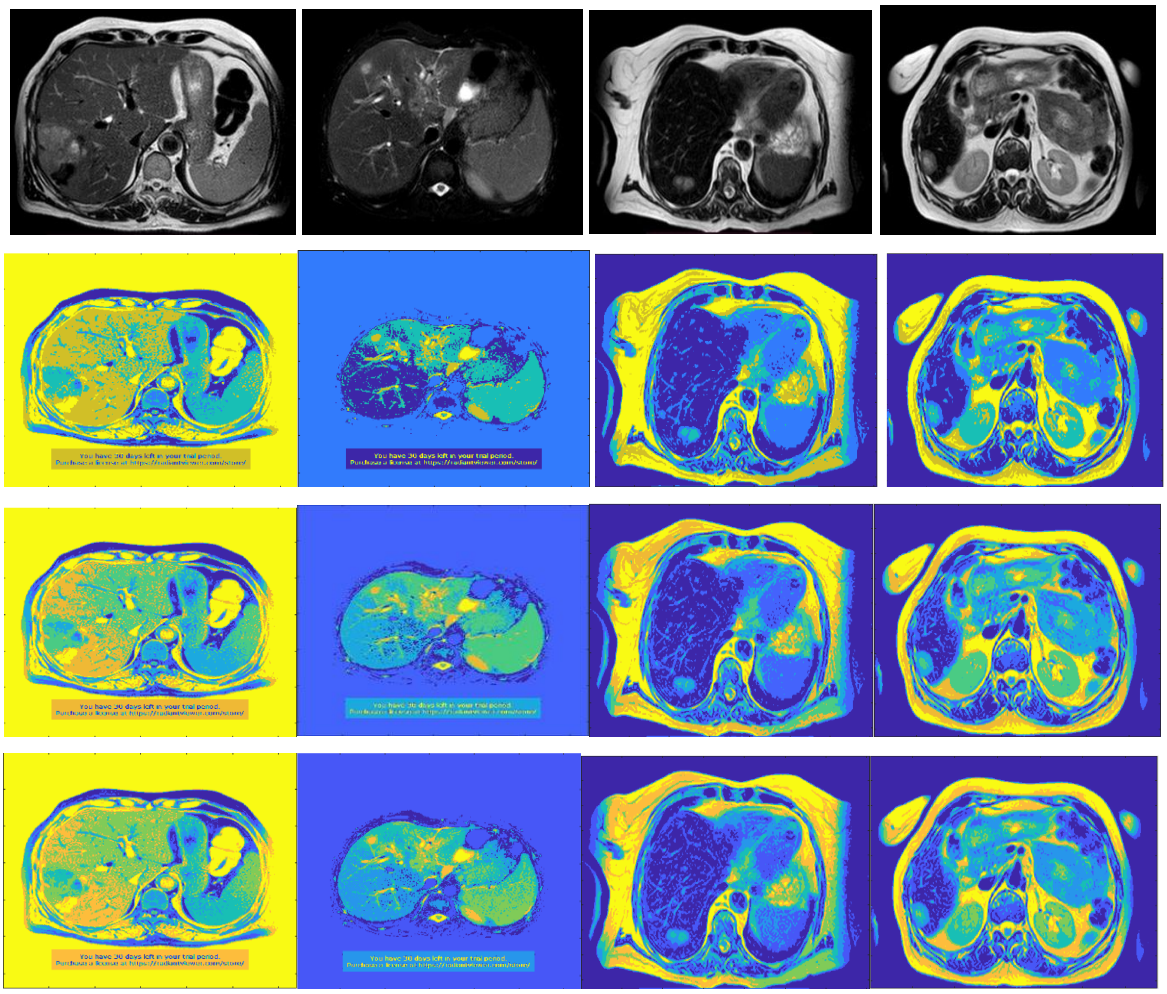

Fig. (4): Results of implementing HSOFM on Im2, Im3, Im4 and Im5 images with five, six and seven nodes (in the current study) .

The final refined abnormal regions were extracted from the segment that the abnormality belongs to, by applying additional processes, opening morphological process of structure element with 'disk shaped' of different radius depending on the extra pixels in each image. Fig. (5) presents these results.

ISSN: 2312-8135 | Print ISSN: 1992-0652
info@journalofbabylon.com | jub@itnet.uobabylon.edu.iq | www.journalofbabylon.com

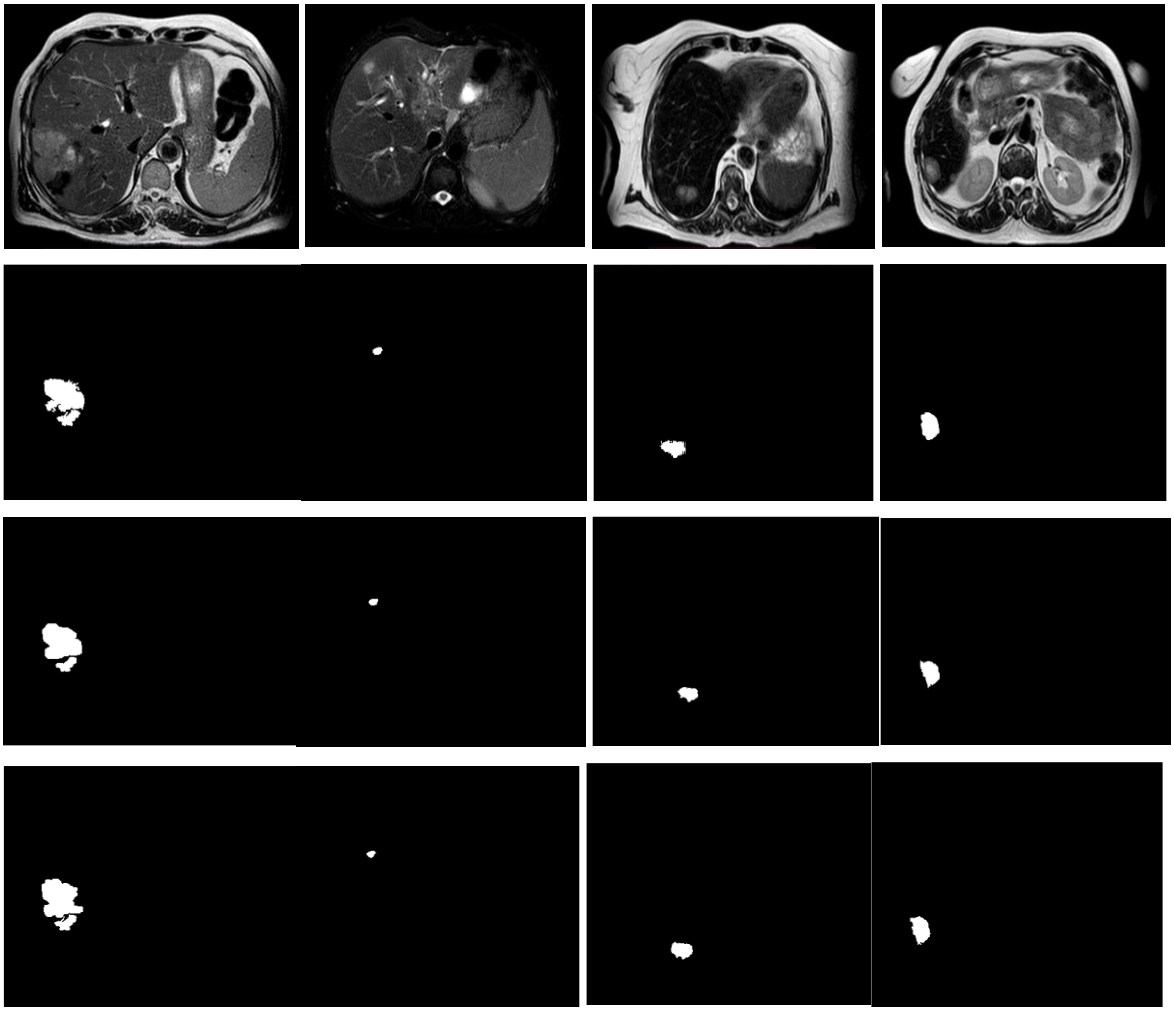

Fig. (5): The refined extracting abnormal regions of Im2, Im3, Im4 and Im5 images for five, six and seven nodes from first line of images to the last one. (in the current study) **.**

6.2 CT scan images

ISSN: 2312-8135 | Print ISSN: 1992-0652
info@journalofbabylon.com | jub@itnet.uobabylon.edu.iq | www.journalofbabylon.com

As for MRI images, HSOFM was applied on four CT scan images, that named **Im11**, **Im22, Im33 and Im44** with different numbers of nodes to figure out the most proper number of nodes. The following figures present the results of clustering and segmenting the adopted images with 4, 5 and 6 nodes.

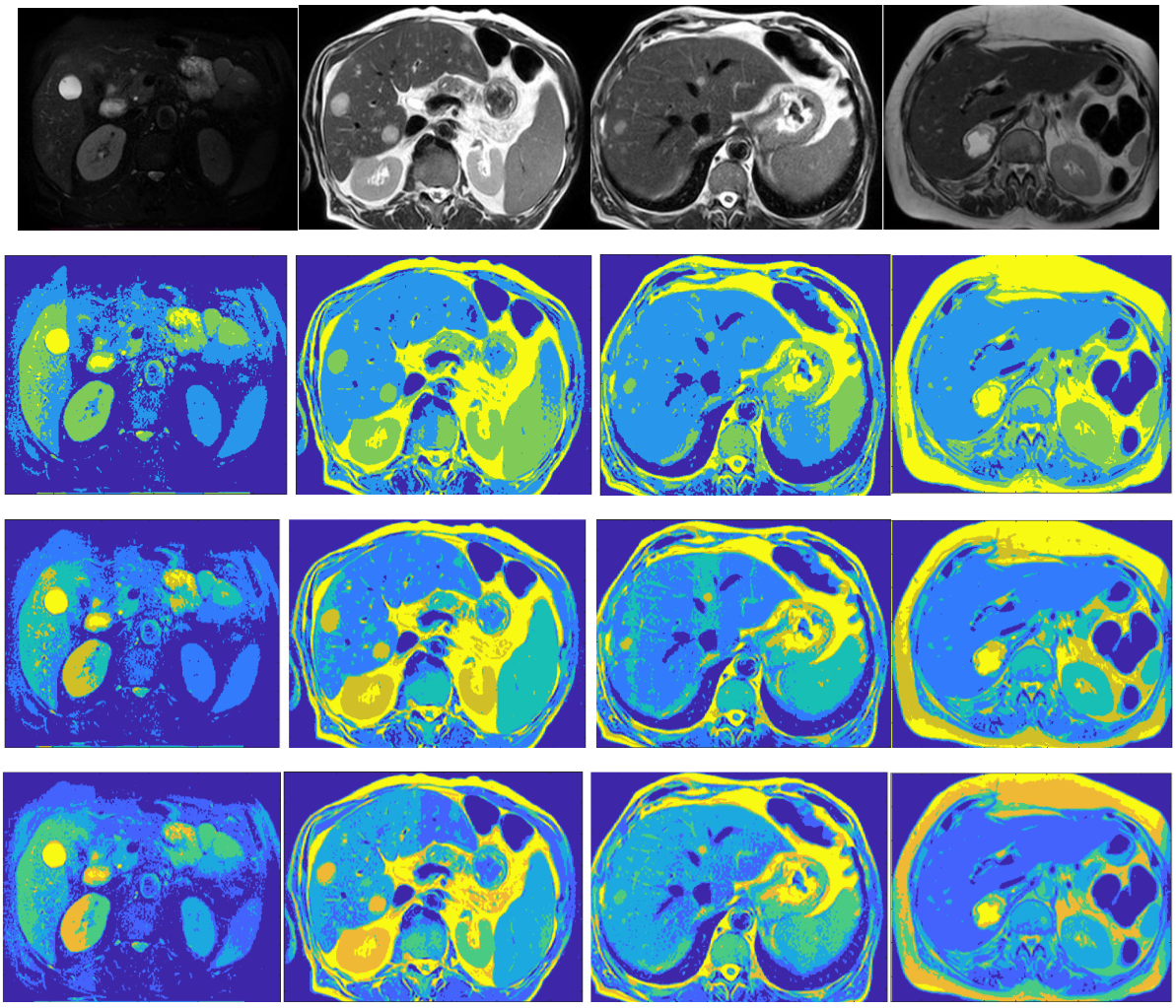

Fig. (6): clustered HSOFM images of Im11, Im22, Im33 and Im44 CT scan with four, five and six nodes (in the current study).

In Fig. (6), first line of images is for the input CT images, while the results segmenting the adopted images with 4, 5 and 6 number of nodes are presented from line two to the last one respectively.

Opening morphological process with a disk shape structure element of proper radius that suitable for each case to get rid and refine the extra pixels that do not belong to the abnormalities, were adopted to the resultant images, the segment that the abnormalities belong

ISSN: 2312-8135 | Print ISSN: 1992-0652
info@journalofbabylon.com | jub@itnet.uobabylon.edu.iq | www.journalofbabylon.com

to. The refined abnormal regions are shown in Fig. (7) for Im**11**, **Im22**, **Im33** and **Im44** CT scan images from the first column to the last one respectively.

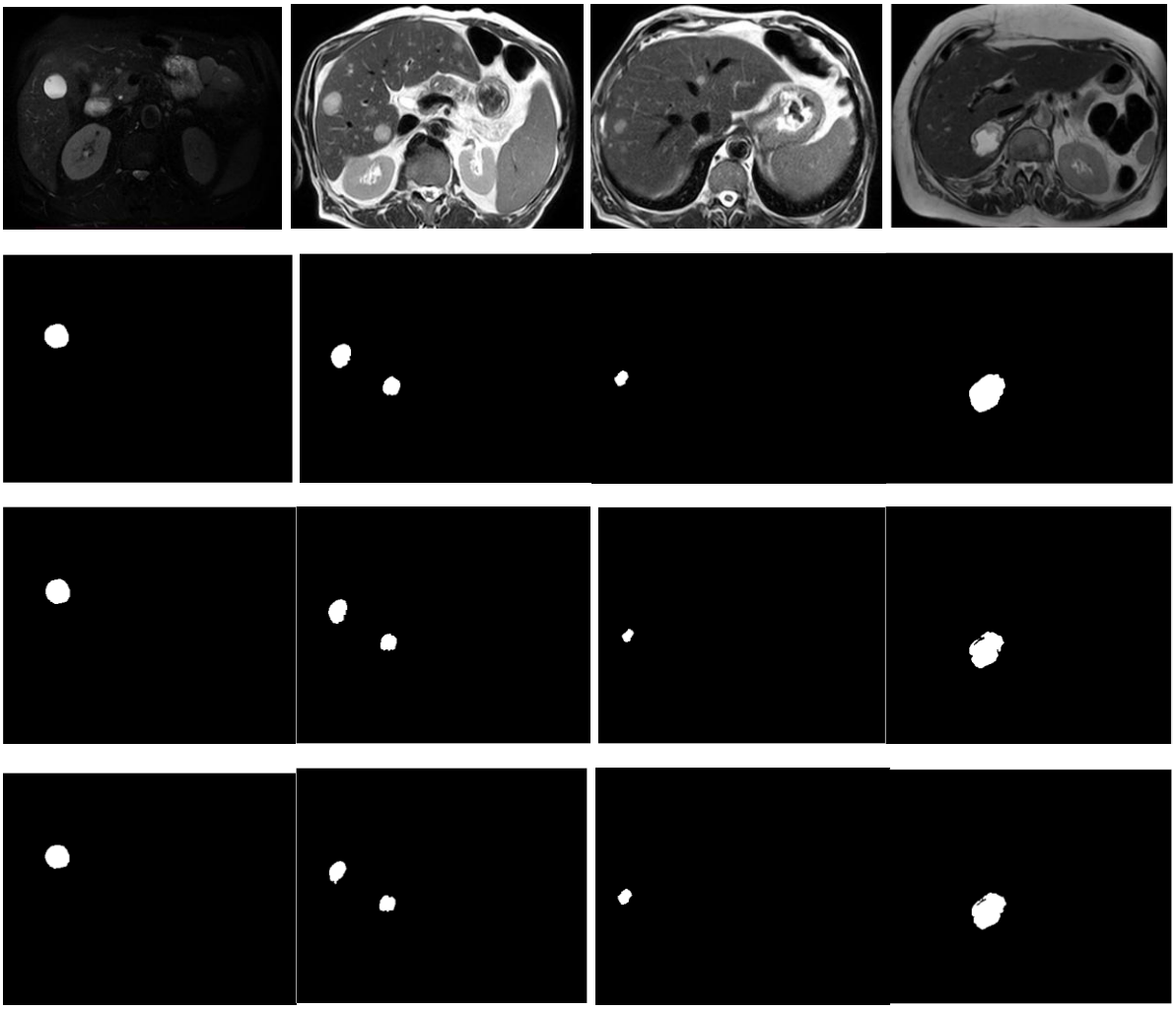

Fig. (7): The refined extracting abnormal regions of Im11, Im22, Im33 and Im44 CT scan images with four, five and six nodes from the first line of images to the last one (in the current study).

6.3 The surface area assessment

In this stage, the final refined abnormal regions surface area, extracted by applying HSOFM, was calculated and the results are presented in Tables (2) and (3) for MRI and CT scan images respectively.

Table (2): Surface area values calculated for the extracted abnormal regions of MRI images with different numbers of nodes.

ISSN: 2312-8135 | Print ISSN: 1992-0652
info@journalofbabylon.com | jub@itnet.uobabylon.edu.iq | www.journalofbabylon.com

Image Name.	Surface area (pixels)		
	Number of nodes		
	five	six	seven
Im1	6117	6342	6329
Im2	6988	7505	7507
Im3	357	328	263
Im4	703	1005	1291
Im5	1790	1627	1630

Table (3): The surface area values of the extracted abnormalities regions for CT scan images with different number of nodes.

Image Name.	Surface Area (pixels)		
	Number of nodes		
	four	five	six
Im11	1575	1536	1491
Im22	1897	1677	1468
Im33	401	275	395
Im44	8619	7297	7614

ISSN: 2312-8135 | Print ISSN: 1992-0652
info@journalofbabylon.com | jub@itnet.uobabylon.edu.iq | www.journalofbabylon.com

6.4 Radiologist delineation

The images under study were submitted to a radiologist for manual delineation of the abnormal regions to get a groundtruth in order to investigate the effeciencity of our proposed technique. Figs.(8) and (9) presented the steps of getting the final abnormal extracted regions of the radiologist delineation.

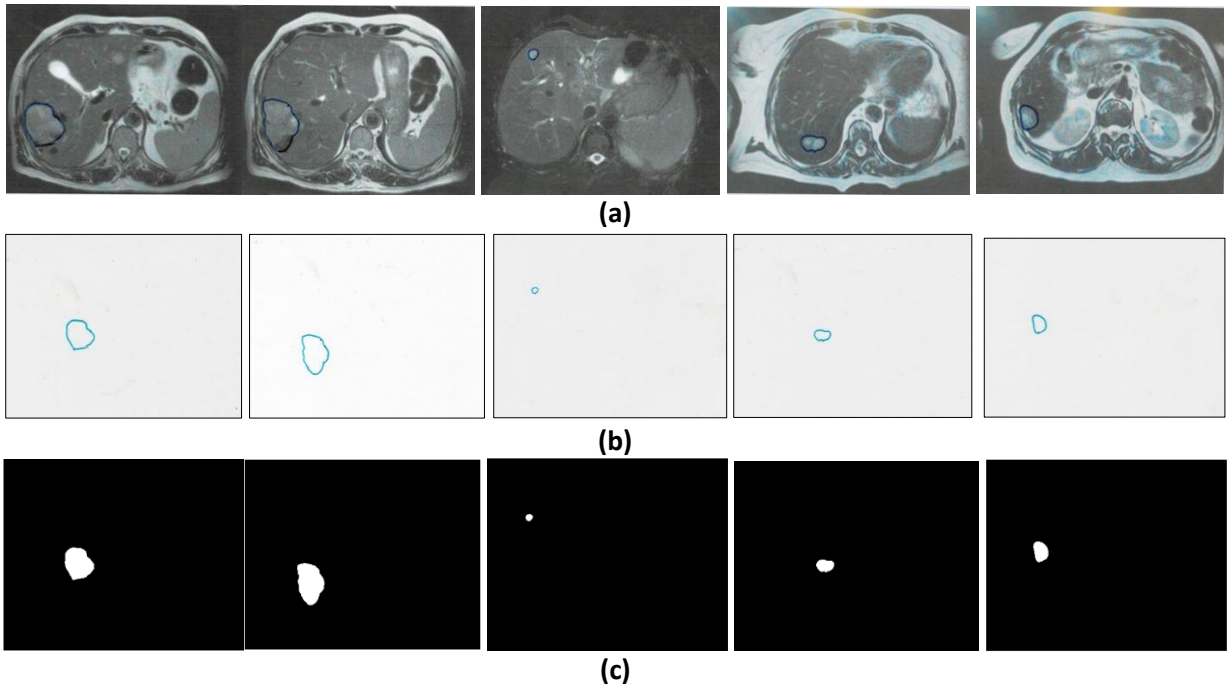

Fig.(8): Radioligist delineation of abnormal areas in MRI images: (a) images with delineation, (b) the contour of abnormalities delineation and (c) the abnormal regions depending on the radiologist's delineating (in the current study).

ISSN: 2312-8135 | Print ISSN: 1992-0652
info@journalofbabylon.com | jub@itnet.uobabylon.edu.iq | www.journalofbabylon.com

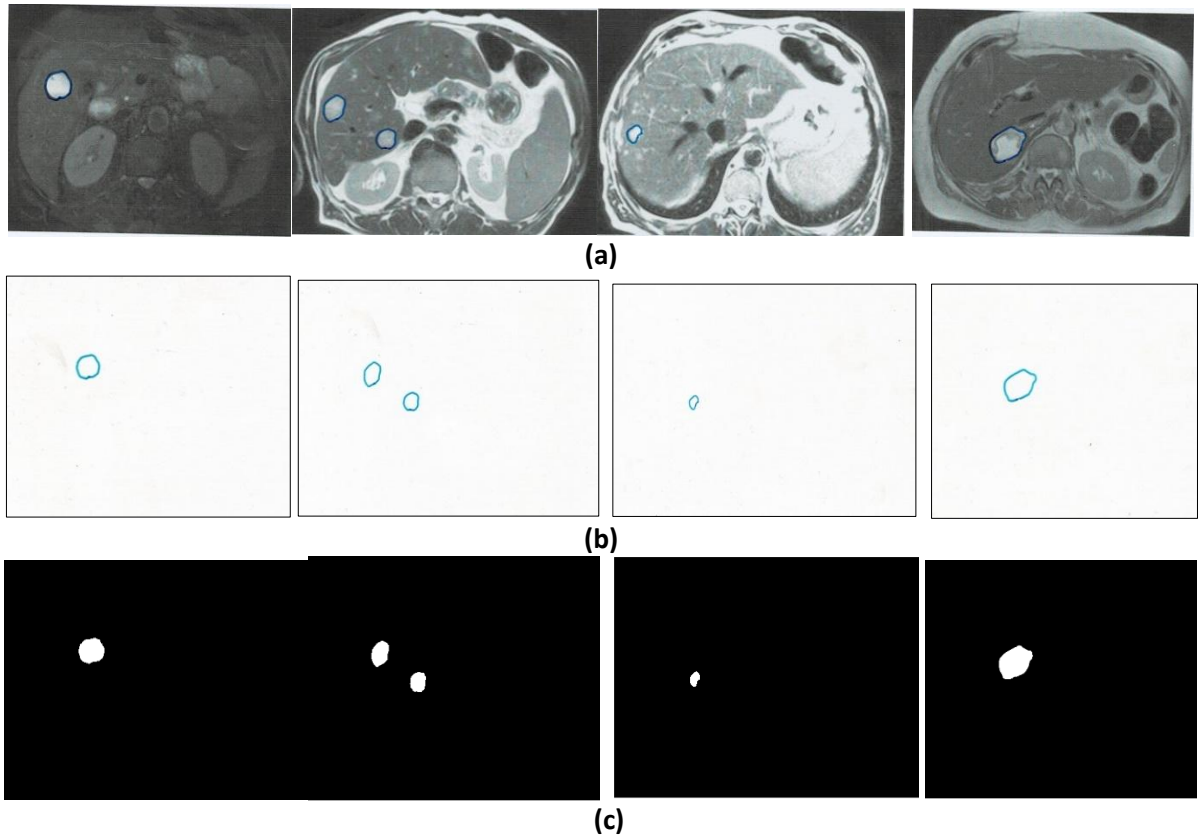

Fig.(10): Radiologist delineation of abnormal areas in CT images:(a) images with delineation, (b) the contour of abnormality delineation and (c) the abnormal regions depending on the doctor's delineating in the current study).

The surface area of the extracted regions in Figs. (8-c) and (9-c) were calculated and presented in the second column of each adopted number of nodes in Tabels (4 and 5). The percent relative differences among them were caculated and presented in Tables (4 and 5).

ISSN: 2312-8135 | Print ISSN: 1992-0652
info@journalofbabylon.com | jub@itnet.uobabylon.edu.iq | www.journalofbabylon.com

Table (4): The percent relative differences of the proposed method and the radiologist for MRI images.

Image Name	Surface area (pixels)						
	radiologist delineation resultant area	Number of nodes					
		five		six		seven	
		HSOFM	relative differense %	HSOFM	relative differenvse %	HSOFM	relative differenvse %
Im1	6200	6117	1.338	6342	2.290323	6329	2.080
Im2	7628	6988	8.390*	7505	1.61248	7507	1.586
Im3	361	357	1.108	328	9.141*	263	27.146*
Im4	1243	703	43.443 *	1005	19.147*	1291	3.861
Im5	1601	1790	11.805*	1627	1.623	1630	1.811
* refers that the number of nodes is not appropriate for the corresponding image.							

Table (5): The percent relative differences of the proposed method and the radiologist for CT scan images.

Image Name	Surface area (pixels)						
	radiologist delineation resultant area	Number of nodes					
		four		five		six	
		HSOFM	relative differense %	HSOFM	relative differenvse %	HSOFM	relative differenvse %
Im11	1591	1575	1.005	1536	3.456	1491	6.285*
Im22	1710	1897	10.935*	1677	1.9298	1468	14.152*
Im33	273	401	46.886*	275	0.732	395	44.688*
Im44	7381	8619	16.772*	7297	1.138	7614	3.156
* refers that the number of nodes is not appropriate for the corresponding image.							

By close inspection of Tabels (4 and 5), it can be concluded that, there is an approporiate number of nodes that is adquate for segmenting each adopted image according to the intensity variance of the component inside each of them. The percent

ISSN: 2312-8135 | Print ISSN: 1992-0652
info@journalofbabylon.com | jub@itnet.uobabylon.edu.iq | www.journalofbabylon.com

relative difference among the results of the implemented method and the work of the radiologist are from 1.108% to 3.861% for MRI images and the range from 0.732 % to 3.456 % for CT scan image. The pereformance accuracy of HSOFM to segment and isolate abnormal regions within adopted liver images was calculated by finding the ratio of segmented images to the total input images, and it was found 95%.

6.5 FCM clustering method

In this step of work, fuzzy c-mean, FCM, an unsupervised clustering method was implemented to investigate its performance and to compare its quality with HSOFM algorithm depending on the percent relative difference. This method was implemented on the same CT scan and MRI images (**Im11, Im22, Im33** and **Im44**), and (**Im1, Im2, Im3 , Im4** and **Im5**) respectively.

6.5.1 The results of CT scan images

FCM method was implemented on the four CT scan images with different numbers of segments to investigate the proper number that enables getting the best isolation of abnormalities. Fig. (11) presents the results of this step with numbers: 3, 2, 4 and 3 of the four images respectively from the first image in the first line to the fourth image in the fourth line.

ISSN: 2312-8135 | Print ISSN: 1992-0652
info@journalofbabylon.com | jub@itnet.uobabylon.edu.iq | www.journalofbabylon.com

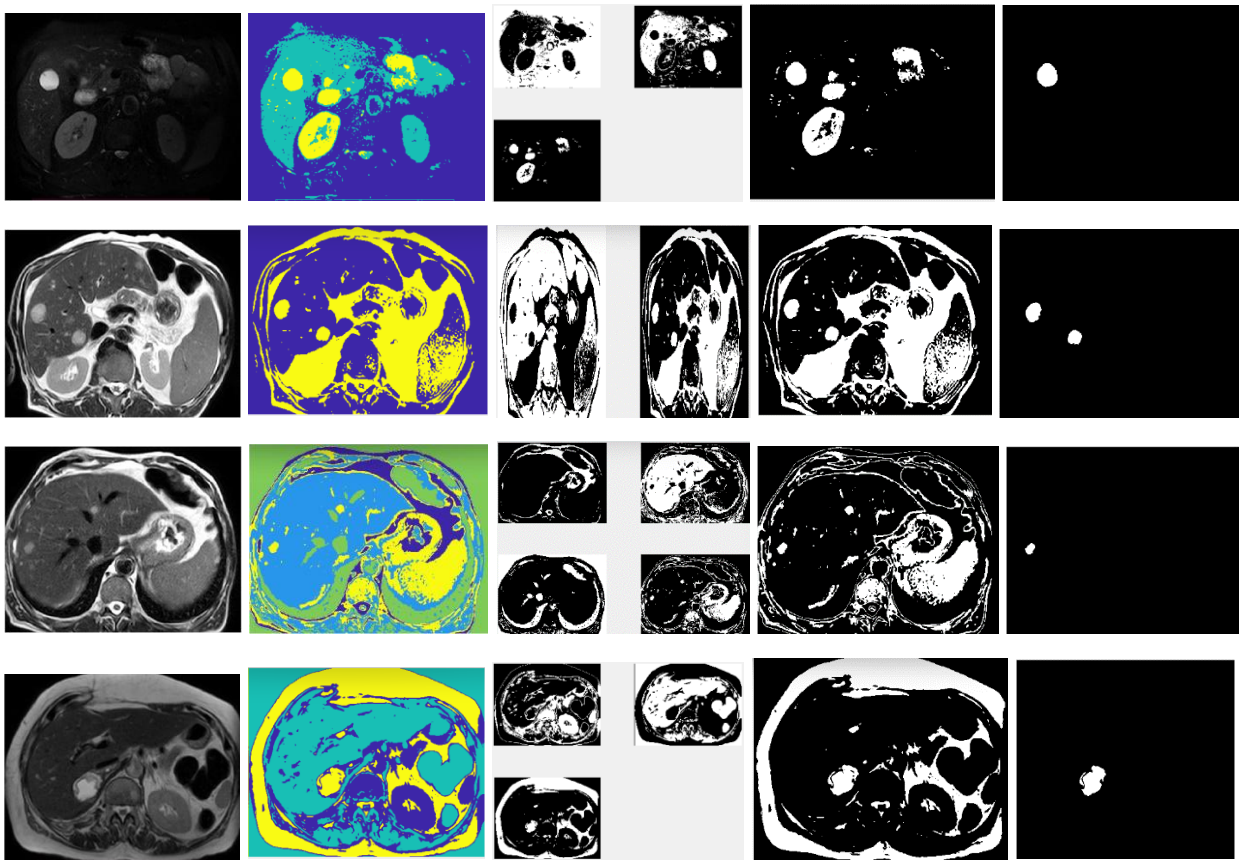

Fig. (11): clustered FCM images of Im11, Im22, Im33 and Im44 CT scan with 3, , 2, 4 and 4 clusters respectively from first line to the last one (in the current study).

In Fig. (11), the input images are in the first column, the clustered images are in the second column, the discrete clusters are in the third column, the fourth column shows the cluster of abnormal regions, while the last column presents the final extracted abnormal region

6.5.2 The results of MRI images

In this section, FCM method was applied to the five MRI images with different number of clusters to investigate the proper number that enable getting the best isolation of abnormalities. Fig. (12) presents the results of this step with cluster numbers: 5, 4, 3, 3 and 3 of the five images respectively from the first image in the first line to the fifth image in the fifth line.

ISSN: 2312-8135 | Print ISSN: 1992-0652
info@journalofbabylon.com | jub@itnet.uobabylon.edu.iq | www.journalofbabylon.com

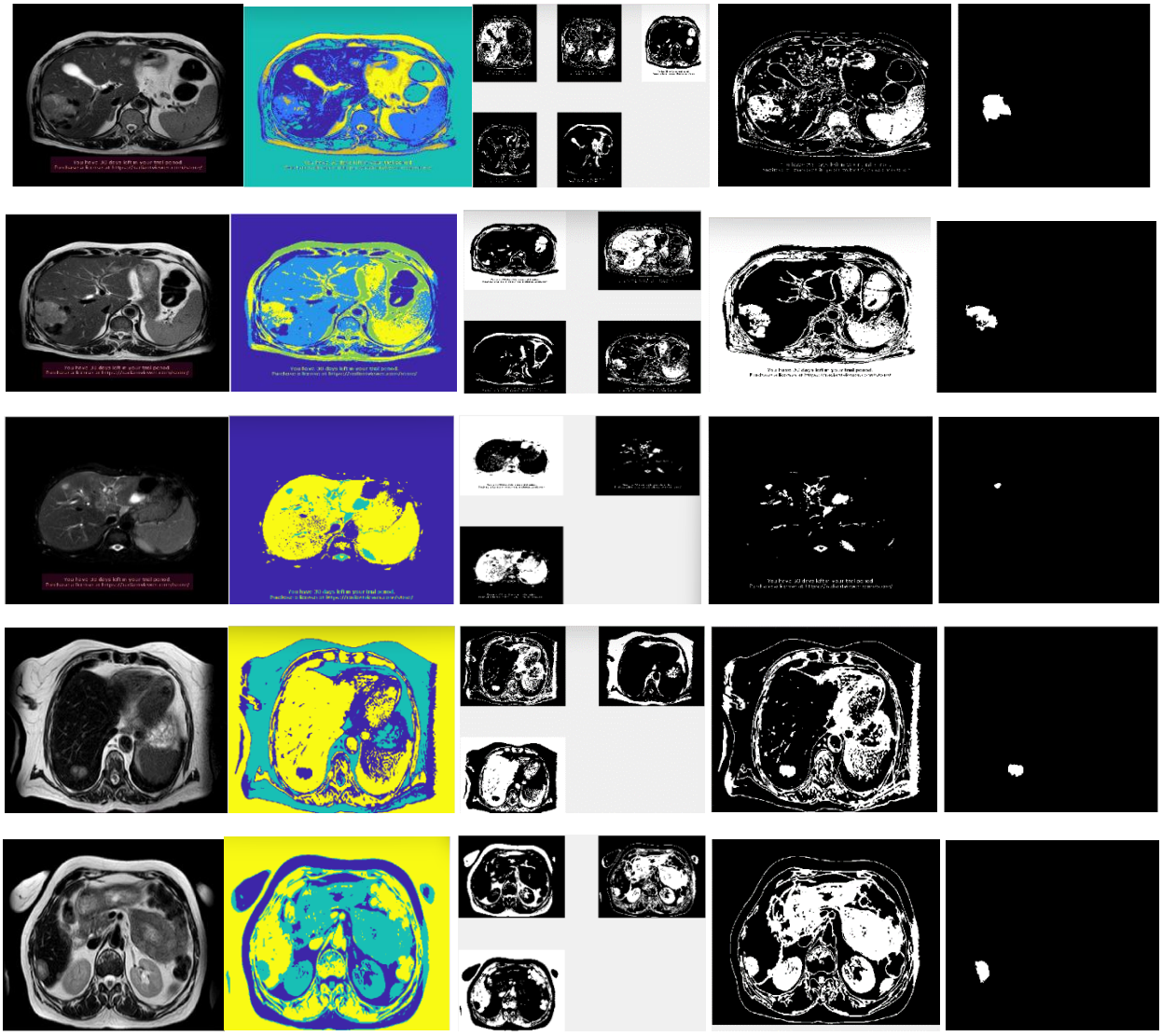

Fig. (12): Clustered FCM images of Im11, Im22, Im3. Im4 and Im5 MRI images with 5, 4, 3, 3 and 3 clusters respectively from first line to the last one (in the current study) .

In Fig. (12), the input images are in the first column, the clustered images are in second column, the discrete clusters are in the third column, the fourth column shows the cluster of abnormal regions, and the last column shows the final extracted abnormal regions.

ISSN: 2312-8135 | Print ISSN: 1992-0652
info@journalofbabylon.com | jub@itnet.uobabylon.edu.iq | www.journalofbabylon.com

The abnormal regions were extracted by implementing FCM with different number of clusters and the clusters numbers: 3, 2, 4 and 3 found the best ones of **Im11, Im22, Im33** and **Im44** CT scan images respectively. The areas of these extracted regions were estimated and the percent relative difference was calculated. Table (6) presents these values with a comparison with results of **HSOFM.**

Table (6): presents a comparison of the surface area values of the abnormal regions of CT scan images by implementing FCM and HSOFM with the proper number of clusters and nodes.

Image Name	Surface area (pixels)				
	radiologist delineation resultant area	CT images			
		HSOFM	relative differense %	FCM	relative differense %
Im11	1591	1575	1.005 (4)	1805	13.450 (3)
Im22	1710	1897	1.9298 (5)	1784	4.327 (2)
Im33	273	401	0.732 (5)	331	21.245* (4)
Im44	7381	8619	1.138 (5)	9379	27.069* (3)
(..) refers to the best number of clusters. *** refers the high relative difference**					

In the same procedure, the abnormal regions were extracted by implementing FCM with different numbers of clusters and the clusters numbers: 5, 4, 3, 3 and 3 found the best ones for **Im1, Im2, Im3**, **Im4** and **Im5** MRI images respectively. The areas of these extracted regions were estimated and the percent relative difference were calculated. Table (7) presents these values with a comparison with results of HSOFM.

ISSN: 2312-8135 | Print ISSN: 1992-0652
info@journalofbabylon.com | jub@itnet.uobabylon.edu.iq | www.journalofbabylon.com

Table (7): presents a comparison of the surfce area values of the abnormal regions of MRI images by implementing FCM and HSOFM with the proper number of clusters and nodes.

Image Name	Surface area (pixels)				
	radiologist delineation resultant area	MRI images			
		HSOFM	relative differense %	FCM	relative differense %
Im1	6200	6117	1.338 (5)	5929	4.370 (5)
Im2	7628	6988	1.586 (7)	4232	44.520* (4)
Im3	361	357	1.108 (5)	264	26.869* (3)
Im4	1243	703	3.861 (7)	1234	0.724 (3)
Im5	1601	1790	1.623 (6)	1623	1.374 (3)

(..) refers to the best number of clusters.
*** refers the high relative difference.**

From the Tables (6 and 7), by implementing FCM clustering, the percent relative difference was in the range from 0.724% to 4.370 % for three MRI images, while for CT scan images, the percent relative difference was 4.327 % for one of the adopted CT images. The comparison among the results of the two implemented methods, HSOFM and FCM, figures out the superiority of HSOFM method over FCM algorithm.

7. DISCUSSION

In this study, HSOFM unsupervised artificial neural network and FCM clustering algorithm were implemented to segment and isolate the abnormalities in MRI and CT scan liver images and extracting the refined regions by the aid of morphological opening operation with different sizes of the adopted disk shape structure element. The findings indicate the high quality performance of HSOFM applied technique with an accuracy of 95%. We can conclude from the results that is an appropriate number of nodes that are more adequate choices than others depending on the properties intensity varians in each processed image. As well as, there is a high agreement with the groundtruth (radiologost delineation) with percent relative difference that ranged from 1.108% to 3.861% for MRI images and ranged from 0.732 % to 3.456 % for CT scan images. By implementing FCM clustering, the percent relative difference was in the range from 0.724% to 4.370 % for three MRI images, while for CT scan images, the percent relative difference was 4.327 % for one of the adopted CT images. The comparison between the two implemented methods HSOFM and FCM figures out the superiority of HSOFM method over FCM.

ISSN: 2312-8135 | Print ISSN: 1992-0652
info@journalofbabylon.com | jub@itnet.uobabylon.edu.iq | www.journalofbabylon.com

8. LIMITATIONS

There are some limitations such as the small size of the abnormal regions that wanted to be extracted as well as the interference of the abnormal regions with the normal regions of the similar intensity that requires applying advanced enhancement methods as addition preprocessing step.

9. CONCLUSIONS

From the results we can conclude that there is an appropriate number of nodes and clusters that is more adequate choice than others depending on the properties intensity varians and other characteristics in each processed image when implementing HSOFM and FCM. The comparison among the two implemented methods figures out the superiority of HSOFM method over FCM with accuracy 95%..

10. RECOMMENDATIONS FOR FUTURE WORKS

Recommendations for future works can be summarized as employing other segmentation methods to compare their performance with HSOFM technique like K-Means, Mean shift, Region growing and watershed to figure out the superiority of them in extracting abnormal regions in medical images of different modalities. As well as, this comparison can be done for different organs images of different images modalities.

ACKNOWLEDGMENT

The authors thank Dr. Karrar O. Al-Mansoori, for his efforts in delineating the regions of the tumor and the authors also extend their thanks to Dr. Roaa Falah Al-Jubawi for her consultations and tumor diagnosis.

ISSN: 2312-8135 | Print ISSN: 1992-0652

info@journalofbabylon.com | jub@itnet.uobabylon.edu.iq | www.journalofbabylon.com

مجلة جامعة بابل للعلوم الصرفة والتطبيقية مجلة جامعة بابل للعلوم الصرفة والتطبيقية

Conflict of interests.

There are non-conflicts of interest.

References

[1] T. Prakash, "Medical image processing methodology for liver tumor diagnosis," *Int. J. Soft Comput.*, vol. 8, no. 3/4, Nov. 2017.

[2] J. C. Wiederkehr, I. M. Coelho, S. G. Avilla, B. A. Wiederkehr, and H. A. Wiederkehr, *Hepatic surgery: Liver tumors in infancy*. 2013, CC BY.

[3] Y. Alvi, D. Regan, L. Schook, R. Gaba, and K. Schachtschneider, "Transcriptional regulation of alcohol induced liver fibrosis in a translational porcine hepatocellular carcinoma model," *Biochimie*, vol. 182, pp. 73–84, Mar. 2021.

[4] R. Naseem et al., "Cross-modality guided contrast enhancement for improved liver tumor image segmentation," *IEEE Access*, vol. 9, pp. 118154–118168, Aug. 2021, doi: 10.1109/ACCESS.2021.3107473.

[5] R. S. Abdoon and K. O. S., "Extracting of liver abnormalities and tumors in medical magnetic resonance imaging and computed tomography scan images," *J. Adv. Microsc. Res.*, vol. 13, pp. 430–450, 2018.

[6] G. Katti, S. A. Ara, and A. Shireen, "Magnetic resonance imaging (MRI) – A review," *Int. J. Dent. Clin.*, vol. 3, no. 1, pp. 65–70, 2011.

[7] A. J. Worth, N. Makris, V. S. Caviness, and D. N. Kennedy, "Neuroanatomical segmentation in MRI: Technological objectives," *Center Morphometric Anal., Gen. Hosp.-East, Charlestown, USA*, 2000.

[8] J. E. K. Newman, F. D. Johnson, T. K. Kirch, and D. L. Kirch, "Abdominal organ segmentation using texture transforms and a Hopfield neural network," *IEEE Trans. Med. Imaging*, vol. 18, no. 7, pp. 640–648, 1999.

[9] C. C. Lee, P. C. Chung, and H. M. Tsai, "Identifying abdominal organs from CT image series using a multimodule contextual neural network and spatial fuzzy rules," *IEEE Trans. Inf. Technol. Biomed.*, vol. 7, no. 3, pp. 208–217, 2003.

[10] K. Mala, V. Sadasivam, and S. Alagappan, "Neural network based texture analysis of liver tumour from computed tomography images," *World Acad. Sci. Eng. Technol. Int. J. Med. Health Biomed. Bioeng. Pharm. Eng.*, vol. 2, no. 1, 2008.

[11] P. Campadelli, E. Casiraghi, and A. Esposito, "Liver segmentation from computed tomography scans: A survey and a new algorithm," *Artif. Intell. Med.*, vol. 45, no. 2–3, pp. 185–196, 2009.

[12] O. Zayane, B. Jouini, and M. A. Mahjoub, "Automatic liver segmentation method in CT images," *Can. J. Image Process. Comput. Vis.*, vol. 2, no. 8, 2011.

[13] M. Jayanthi and B. Kanmani, "Extracting the liver and tumor from abdominal CT images," in *Proc. 5th Int. Conf. Signal Image Process. (ICSIP)*, 2014, IEEE.

[14] R. S. Abdoon and K. O. S., "Employing histogram equalization enhancement technique to segment different medical images of three organs," *J. Adv. Microsc. Res.*, vol. 13, pp. 494–502, 2018.

[15] A. A. Hussein and R. S. Abdoon, "Clustering based artificial neural network to isolate COVID-19 infected lung regions," *J. Optoelectron. Laser*, vol. 41, no. 4, pp. 260–274, 2022.

[16] A. A. Hussein and R. S. Abdoon, "Utilizing clustering FCM and contrast based enhancement to isolate COVID-19 infected regions in CT lung images," *HIV Nurs.*, vol. 23, no. 1, pp. 804–808, 2023.

[17] E. A. Salman, R. S. Abdoon, and L. E. George, "Simulating the tumor mass changes in PET and PET/CT segmented images using unsupervised artificial neural network," *Math. Model. Eng. Probl.*, vol. 11, no. 8, pp. 2243–2250, Aug. 2024.

[18] W. E. Reddick, J. O. Glass, and E. N. Cook, "Automated segmentation and classification of multispectral magnetic resonance images of brain using artificial neural networks," *IEEE Trans. Med. Imaging*, vol. 16, pp. 911–918, 1997.

[19] T. Kohonen, *Self-organization and associative memory*. New York: Springer-Verlag, 1989.

[20] S. A. Mingoti and J. O. Lima, "Comparison SOM neural network with fuzzy C-means, K-means and traditional hierarchical clustering algorithms," *Eur. J. Oper. Res.*, vol. 17, pp. 1742–1759, 2006.

[21] A. Krenker, J. Bešter, and A. Kos, "Introduction to the artificial neural networks," in *Artificial neural networks-methodological advances and biomedical applications*, K. Suzuki, Ed., 2011.

[22] T. Logeswari and M. Karnan, "An improved implementation of brain tumor detection using segmentation based on soft computing," *J. Cancer Res. Exp. Oncol.*, vol. 2, no. 1, pp. 6–14, 2010.

[23] M. J. Moghaddam and H. Soltanian-Zadeh, "Medical image segmentation using artificial neural networks," in *Artificial neural networks-methodological advances and biomedical applications*, K. Suzuki, Ed., InTech, 2011.

[24] J. B. MacQueen, "Some methods for classification and analysis of multivariate observations," in *Proc. 5th Symp. Math., Statist., Probab.*, Berkeley, CA: Univ. California Press, 1967, pp. 281–297.

[25] G. G. N. Geweid, M. A. Abdallah, and A. M. Hassan, "Improved malignant diagnosis using fuzzy C-means based on histopathological of PET-CT lung images," 2020.

[26] F. Hoseini and G. M. Dekahi, "High-performance implementation of fuzzy C-means and watershed algorithms for MRI segmentation," *J. Adv. Comput. Res.*, vol. 10, no. 1, 2019.

[27] A. Meena and K. Raja, "Spatial fuzzy C-means PET image segmentation of neurodegenerative disorder," *Indian J. Comput. Sci. Eng.*, vol. 4, no. 1, 2013.

[28] J. C. Bezdek, *Pattern recognition with fuzzy objective function algorithms*. New York: Plenum Press, 1981.

[29] D. Q. Zhang, S. C. Chen, Z. S. Pan, and K. R. Tan, "Kernel-based fuzzy clustering incorporating spatial constraints for image segmentation," in *Proc. Int. Conf. Mach. Learn. Cybern.*, vol. 4, 2003, pp. 2189–2192.

[30] P. Maragos and R. W. Schafer, "Morphological filters—Part I: Their set theoretic analysis and relations to linear shift–invariant filters," *IEEE Trans. Acoust., Speech, Signal Process.*, vol. ASSP-35, pp. 1153–1169, 1987.

ISSN: 2312-8135 | Print ISSN: 1992-0652
info@journalofbabylon.com | jub@itnet.uobabylon.edu.iq | www.journalofbabylon.com

[31] T. Kapur, E. W. L. Grimson, W. M. Wells, and R. Kikinis, "Segmentation of brain tissue from magnetic resonance images," *Med. Image Anal.*, vol. 1, no. 1, pp. 109–127, 1996.

[32] S. Tiwari, A. B., and R. S., "Identification of brain tumors in 2D MRI using automatic seeded region growing method," *J. Educ.*, vol. 2, no. 1, pp. 41–43, 2012.

ISSN: 2312-8135 | Print ISSN: 1992-0652
info@journalofbabylon.com | jub@itnet.uobabylon.edu.iq | www.journalofbabylon.com

ISSN: 2312-8135 | Print ISSN: 1992-0652
info@journalofbabylon.com | jub@itnet.uobabylon.edu.iq | www.journalofbabylon.com

الخلاصة

المقدمة: ورم الكبد مرض خطير قد يؤدي إلى الوفاة، وتزداد فرص النجاة عند اكتشافه مبكرًا

طرق العمل: في هذه الدراسة، تم استخدام أسلوب التجميع Fuzzy c-mean و "Self-Organization Feature Map" وHSOFM، وهي شبكة عصبية اصطناعية غير خاضعة للإشراف معتمدة على المخطط التكراري للصورة، لغرض تجزئة الصورة وعزل الأورام والمناطق غير الطبيعية الأخرى ثم استخراجها من صور الرنين المغناطيسي والتصوير المقطعي المحوسب للكبد. تم استخدام عمليات معالجة اضافية ومنها العمليات المورفولوجية لتحقيق الاستخراج النهائي الكامل للمناطق المعزولة دون أي بكسلات إضافية لا تنتمي إلى المناطق غير الطبيعية. تم تطبيق هاتين الطريقتين على خمس صور بالرنين المغناطيسي وأربع صور بالتصوير المقطعي المحوسب. حسبت المساحات السطحية للمناطق المستخرجة ومقارنتها بمناطق الكتل الحقيقية المستخرجة يدويًا من قبل طبيب الاشعة للتحقق من مدى جودة الطرق المتبعة. تم تنفيذ العمل باستخدام البيئة البرمجية الماتلاب .

النتائج: تراوحت الفروقات النسبية المئوية للمناطق الغير طبيعية المستخرجة باستخدام الطرق المعتمدة مع القيمة الحقيقة الاساسية ما بين 1.108% و3.861% لصور الرنين المغناطيسي، بينما تراوحت نسب الفروقات النسبية لصور الأشعة المقطعية بين 0.732% و3.456%. وبطريقة FCM تراوحت نسب الفروقات النسبية بين 0.724% و4.370% لثلاث صور رنين مغناطيسي، بينما بلغت نسبة الفروقات النسبية لصور الأشعة المقطعية 4.327% لإحدى الصور المستخدمة. تشير نتائج تطبيق طريقة HSOFM إلى جودة أداء عالية لهذه الطريقة بدقة 95%.

الاستنتاجات: من خلال النتائج يمكننا ان نستنتج ان هناك عددا مناسبا من العقد والعناقيد التي تعد خيار اكثر ملائمة من غيرها اعتمادا على خصائص تنوع الشدة لكل صورة قيد المعالجة . تُظهر المقارنة بين الطريقتين المُطبقتين تفوق طريقة HSOFM على FCM. وتوجد بعض القيود منها صغر حجم المناطق الغير طبيعية وكذلك التداخل ما بين بعض المناطق الطبيعية مع المناطق الغير طبيعية التي تشابهها في الشدة لذا يتطلب استخدام طرق تحسين مطورة تستخدم كخطوة معالجة ابتدائية .

الكلمات المفتاحية: **تشوهات الكبد، التجميع الضبابي**، خريطة **الميزات ذاتية التنظيم الهجينة، التصوير بالرنين المغناطيسي، التصوير المقطعي المحوسب.**